Available online at www.sciencedirect.com
ScienceDirect
Trans. Nonferrous Met. Soc. China 33(2023) 2001−2013
Transactions of Nonferrous Metals Society of China
www.tnmsc.cn

Enhancement of strength and ductility in 6061Al alloy processed by cross accumulative roll bonding

Ling OU[1], Lin-yan LI[1], Cai-he FAN[1,2], Yu-feng NIE[3], Jian-jun YANG[1]

1. School of Materials and Advanced Manufacturing, Hunan University of Technology, Zhuzhou 412007, China;
2. Anhui Jianye Science and Technology Co. Ltd., Huaibei 235000, China;
3. School of Mechanical Engineering, Hunan University of Technology, Zhuzhou 412007, China

Received 5 March 2022; accepted 31 May 2022

Abstract: To achieve a good match between strength and ductility, plates of 6061 Al alloy were prepared by cross accumulative roll bonding (CARB) at ambient temperature for up to 7 cycles. The microstructures were analyzed by X-ray diffraction, transmission electron microscopy, scanning electron microscopy and electron backscatter diffraction. The results show that both the ultimate tensile strength and elongation of the CARB specimens are significantly better than those of ARB. Grain size of the samples processed by CARB is smaller, and more low-angle grain boundaries transform into high-angle grain boundaries. Also, the dislocation density in the CARB sample is higher. The rolling texture of the 6061 Al alloy processed by CARB is obviously weakened, and the Brass {011}⟨211⟩ texture is the main one. The higher strength of CARB 6061 Al alloy is mainly dominated by fine grain strengthening and dislocation strengthening, while the higher ductility is due to the finer grains and weak texture.
Key words: cross accumulative roll bonding (CARB); 6061 Al alloy; electron backscatter diffraction (EBSD); crystallographic texture; tensile mechanical properties

1 Introduction

Nanocrystalline and sub-micron ultrafine grained metal materials have fine grain sizes and unique defect structures, and exhibit high ultimate tensile strength, hardness, fatigue life, and super-plasticity at low temperature and high speed. They have attracted great attention from domestic and foreign scholars. Severe plastic deformation (SPD) is the main method used to produce nanocrystalline and submicron ultrafine materials. SPD produces high-density dislocations that are transformed into low-angle grain boundaries (LAGBs) and high-angle grain boundaries (HAGBs) during further processing to prepare ultra-fine grains. It includes equal channel angular pressing (ECAP), high pressure torsion (HPT), simple shear extrusion and accumulative roll bonding (ARB). Among these processes, the ARB process developed by SAITO in 1998 [1] has attracted the interest of scholars. ARB process can achieve a large reduction, breaking the limitations of traditional rolling reduction, and can be used to prepare ultra-fine grained materials for ultra-thin plates. This process has been successfully applied to the production of a variety of alloys and dissimilar metal layered composite materials [2−7], and is considered to be the most promising SPD technology for large-scale production and commercialization.

Plasticity of aluminum alloy plates produced by ARB is significantly decreased [8,9]. It has been a long-term goal of aluminum alloys to achieve both high strength and good ductility [10]. In recent years, scholars have carried out research into the improvement of the plasticity of aluminum alloys

Corresponding author: Cai-he FAN, Tel: +86-731-22183432, E-mail: 369581813@qq.com
DOI: 10.1016/S1003-6326(23)66239-9

processed by ARB. LI et al [11] found that the high ductility of the alloy produced by hot rolling at high strain rate was mainly due to the high content of solute Mg atoms, high fraction of fine grains with HAGBs and the weak texture. NASERI et al [12] studied a unique stacking method to make 2024 Al alloy processed by ARB form a bimodal grain distribution. Compared with the conventional stacking method, the elongation of the samples is improved by this method. In order to further improve the plasticity of the materials, several researchers have discussed the influence of different accumulative rolling methods on the structure and properties of materials. In the ARB process, after each cycle of rolling, the plate is rotated by 90° around the normal direction (ND). This process is called cross accumulative roll bonding (CARB). NASERI et al [13] successfully used CARB to prepare AA1050 aluminum alloy with higher strength and ductility. Electron back scattered diffraction (EBSD) analysis showed that the materials processed by CARB have better overall performance than those of processed by ARB. The grains are finer and more uniform.

6061 Al alloy has good formability and good corrosion resistance, and is widely used in military, aerospace and civil applications. 6061 Al alloy with excellent formability is suitable for production by ARB. In order to achieve a good balance between strength and ductility, CARB is used to produce 6061 Al alloy sheets with ultrafine grained structure. Compared with the ARB process, the effect of the CARB process on the structure and mechanical properties of 6061 Al alloy is studied systematically.

2 Experimental

The chemical compositions of the 2 mm-thick commercial 6061-T6 aluminum alloy sheets used in the experiment are given in Table 1.

Table 1 Chemical compositions of 6061 Al alloy (wt.%)

Al	Si	Cu	Mg	Zn	Mn	Ti	Gr	Fe
97.54	0.43	0.21	0.93	0.07	0.10	0.13	0.23	0.36

The 6061 Al sheets (80 mm × 60 mm × 2 mm) were solution treated (ST) at 773 K for 1 h, immediately quenched in water to room temperature, and then deformed by ARB or CARB at room temperature for up to 7 cycles, reducing the thickness by 50% in each pass. The schematic illustration of ARB and CARB is shown in Fig. 1. The rolling speed in ARB and CARB was 18.3 m/s without lubricant. The rolled plate was cut into two equal parts and superimposed, and then the rolling was continued according to the aforementioned method. In the second cycle of the CARB process, the laminated plates were rolled after rotating them by 90° around the ND of the rolling surface. Then, they were rotated by 90° for each cycle according to this method. This process was repeated up to the seventh pass.

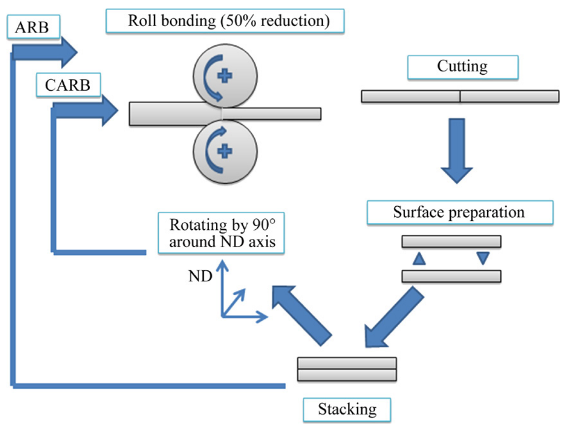

Fig. 1 Schematic illustration of rolling process

The hardness of all samples processed by ARB or CARB was measured using a Leica Vickers microhardness tester. The test load was set at 1.98 kN and the dwell time was 15 s. Tensile tests were performed on SUST CMT5504 at the tensile speed of 1 mm/min. The dimensions of tensile specimens are shown in Fig. 2. Three parallel samples were taken for each cycle. Tensile fracture observation was performed on a scanning electron microscope (SEM; JSM 6510).

The macrotexture on the rolling direction−transverse direction (RD−TD) plane of the sheets was measured by X-ray diffraction (XRD). The

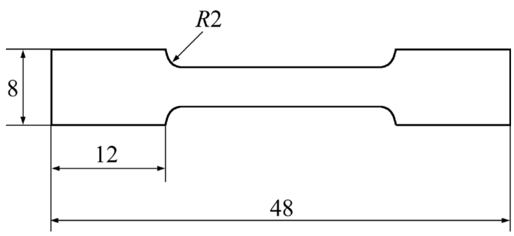

Fig. 2 Dimensions of tensile specimen (unit: mm)

tube voltage was 40 kV and the tube current was 30 mA. The global texture measurements were performed using a Panalytical X'Pert3 MRD X-ray diffractometer. The {111}, {200} and {220} pole figures were scanned using the Schulz back reflection method. The orientation distribution function was obtained by the Bunge series expansion method. The microstructure of the sample was characterized using the Symmetry EBSD detector of Oxford Instruments on a JSM−7900F thermal field emission scanning electron microscope. The samples were measured on the RD−TD plane. The selected area was 120 μm × 50 μm, and the step size was 0.12 μm. The mechanically-polished specimens were thinned subsequently by twin jet electro-polishing in 30% nitric acid and 70% methanol solution at −30 °C, and examined in a JEOL−2100 high resolution transmission electron microscope (HRTEM) operated at 200 kV. The samples were measured on the rolling direction−normal direction (RD−ND) plane.

3 Results

3.1 Mechanical properties

3.1.1 Microhardness

After the solution-treatment and quenching, the microhardness of the 6061 Al plate processed by ARB and CARB varies with increasing the number of cycles, as shown in Fig. 3. As the number of cycles increases, the surface micro-hardness of the 6061 Al sheet increases. From the 5th cycle, the increase in hardness slows down. The rolling direction is changed from the second cycle

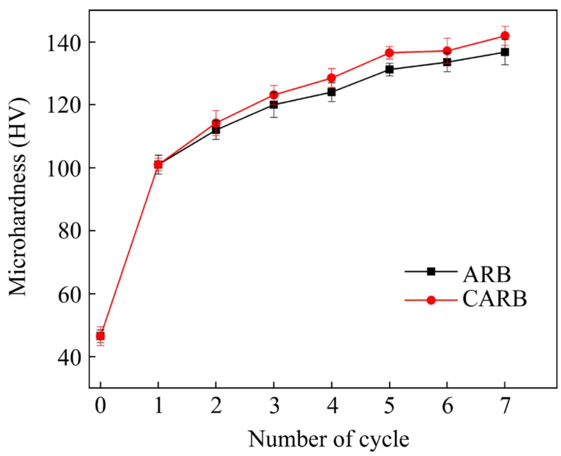

Fig. 3 Variations in microhardness versus number of ARB and CARB cycles

of CARB. The hardness of the plate during this process is higher than that of ARB.

3.1.2 Tensile properties

Figure 4 shows the tensile stress−strain curves of ARB and CARB 6061 Al plate samples. It can be seen that the UTS of the 7-cycle ARB sample is 412 MPa and the elongation is 9.9%. The UTS of the 7-cycle CARB sample is 458 MPa and the elongation is 12.1%. Compared with the tensile properties of 6061-T6 aluminum alloy sheets (234 MPa, 15.7%), the UTS of 6061 Al sheets processed by ARB or CARB is greatly improved, but the elongation is reduced. Among them, the UTS of the 7-cycle CARB specimen increases by 95.7% compared with that of 6061-T6 aluminum alloy specimen.

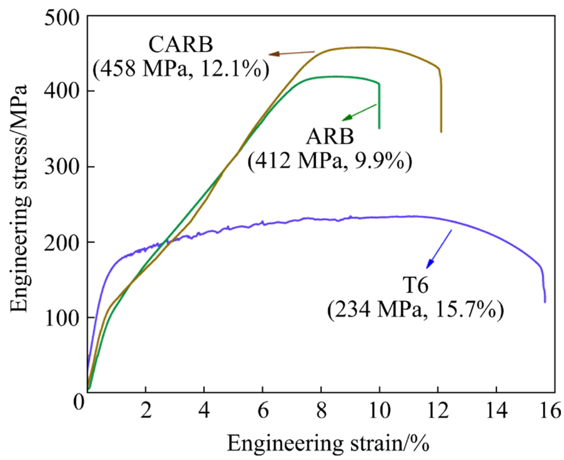

Fig. 4 Typical engineering stress−strain curves of 7-cycle ARB and CARB 6061 Al sheet, and 6061-T6 Al sheet samples

By comparing the tensile stress−strain curves of the 7-cycle 6061 Al alloys processed by ARB and CARB, the UTS and elongation of the CARB 6061 Al sheet are significantly higher than those of ARB. Compared with the ARB specimen, the UTS of the CARB sample increases by 11.2% and the elongation increases by 22.2%. As a result, both the strength and the plasticity of the alloy subjected to CARB are improved.

Figure 5 shows tensile fracture morphologies of the 6061 Al sheet at different states. It can be seen from Fig. 5(a) that deep dimples appear in the fracture of the 6061-T6 aluminum alloy sheets, and the fracture mode is a typical ductile fracture. It can be seen from Figs. 5(b, c) that there are also a large number of dimples in the fracture images of 7-cycle ARB and CARB Al sheet samples. The fracture is

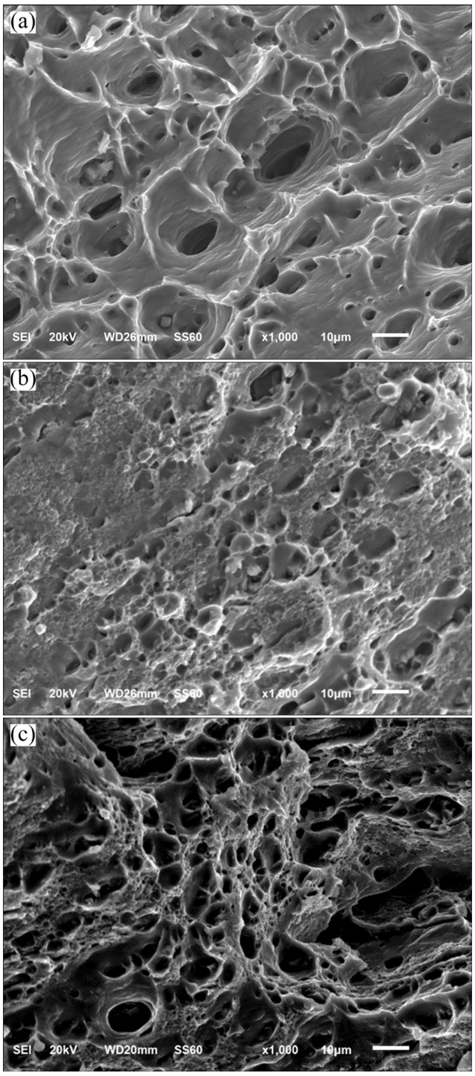

Fig. 5 Tensile fracture morphologies of 6061 Al sheet samples at different states: (a) T6; (b) 7-cycle ARB; (c) 7-cycle CARB

proceeded by the formation of micropores, coarsening, and finally spreading through whole sample. By comparing Figs. 5(a−c), it is found that the 6061-T6 aluminum alloy sheet has the best plasticity and the fracture dimples are deeper than those of ARB and CARB. In addition, the tensile fracture dimples of CARB are deeper and more numerous, indicating that the plasticity of CARB alloy is better than that of ARB. This result is consistent with the aforementioned elongation results.

3.2 Microstructure

3.2.1 Texture

Figure 6 shows the {111}, {200}, {220} polar figures of the 7-cycle ARB and CARB specimens. It can be seen from Figs. 6(a−c) that the main texture orientations of the ARB are Copper {112}⟨111⟩, S {123}⟨634⟩ and Brass {011}⟨211⟩ with the maximum density of 7.1, 4.8 and 2.3, respectively. There are three strong texture orientations in the ARB sample, because rolling along the same direction increases the density of texture orientation. From Figs. 6(d−f), the main texture orientations of the CARB sample are Brass {011}⟨211⟩, S {123}⟨634⟩ and Copper {112}⟨111⟩ with the maximum density of 7.6, 1.6 and 1.2, respectively.

A detailed analysis of the textural evolution can be conducted by ODFs. The ODF plots separate the components that partially overlap in the pole figures, allowing clearer unambiguous comparison of the individual components and fibers. The texture evolution of the 7-cycle ARB and CARB specimens is explained by ODFs, as shown in Fig. 7. The textural components of ARB can be characterized as Copper {112}⟨111⟩, S {123}⟨634⟩, and Brass {011}⟨211⟩ components with maximum indensities of 13.9, 8.2 and 6.7, respectively (Fig. 7(a)). In addition, there are some Goss {011}⟨100⟩ texture components. In the CARB processed specimens (Fig. 7(b)), the maximum indensities of Brass {011}⟨211⟩, Copper {112}⟨111⟩ and S {123}⟨634⟩ components are 20.6, 2.3 and 3.5, respectively. It should be noted that Brass {011}⟨211⟩ component of the CARB specimen deviates significantly from the standard position. The samples tested in the experiments in this work are close to the subsurface and are subjected to shear stress, which causes the texture components to deviate from the ideal position.

In comparison, the β-fiber of the CARB sample is mainly concentrated in Brass {011}⟨211⟩, while the β-fiber of the ARB sample has a more uniform texture distribution. In other words, the Copper {112}⟨111⟩ and S {123}⟨634⟩ rolling texture components are significantly weakened in the CARB sample.

3.2.2 EBSD results

The orientation and corresponding grain boundary maps of the 7-cycle ARB and CARB specimens are shown in Fig. 8. These images were recorded on RD−TD planes. During ARB and CARB, the grains are pulled towards the RD. In addition, the grains are mostly oriented in ⟨101⟩ direction. In Figs. 8(a, b), the colors within the

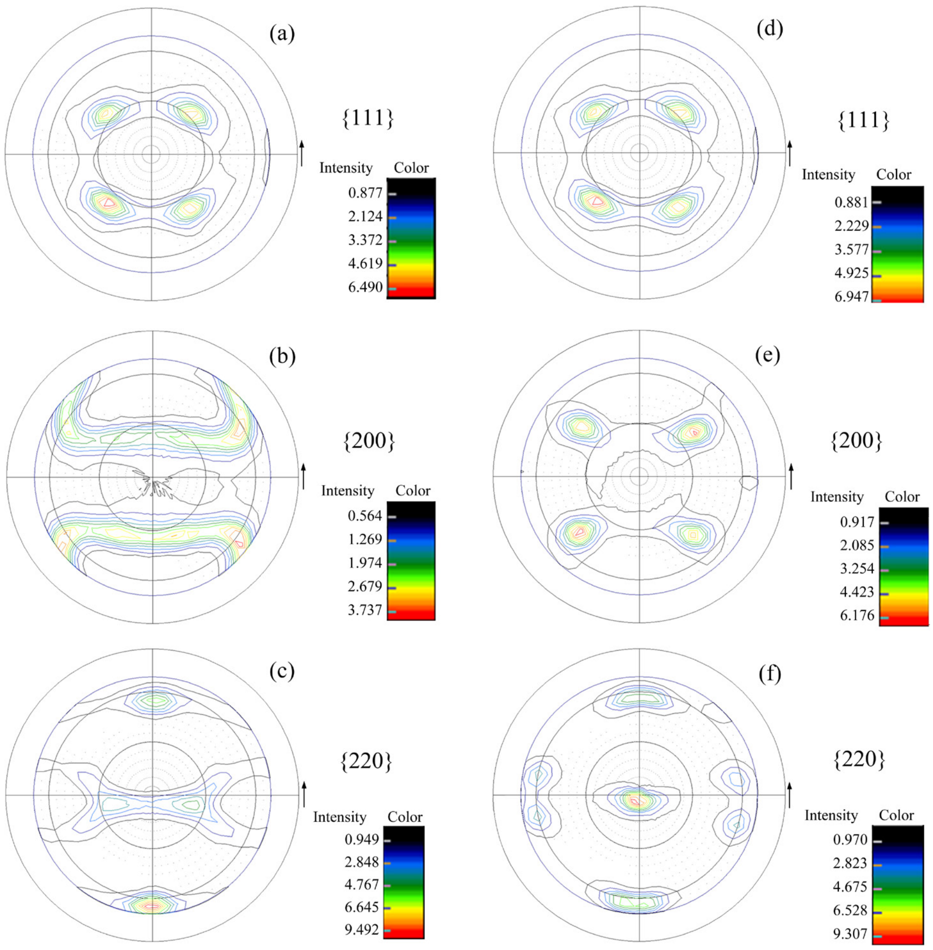

Fig. 6 Pole figures of different crystal planes of sample: (a−c) 7-cycle ARB; (d−f) 7-cycle CARB

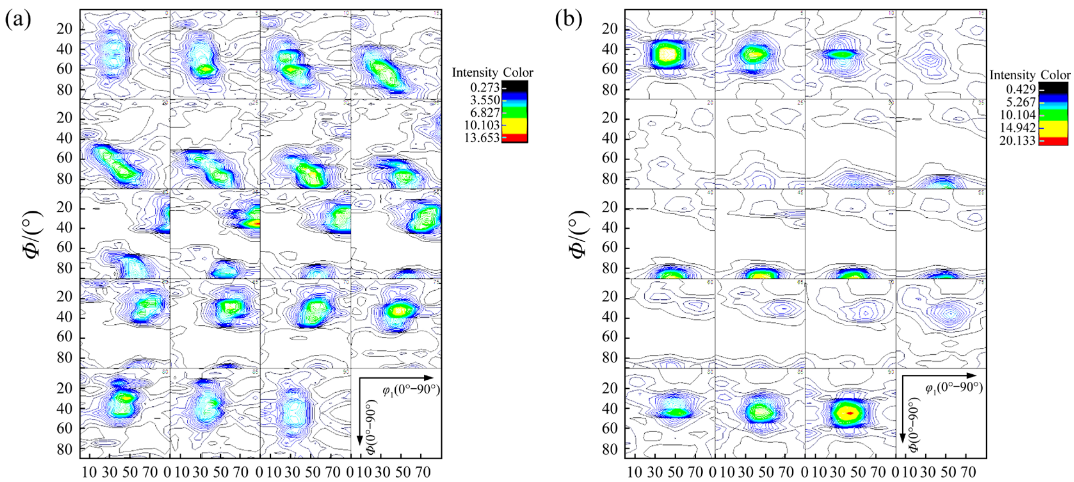

Fig. 7 ODF sections of constant φ_2 showing texture components in 7-cycle ARB (a) and 7-cycle CARB (b) specimens

grains correspond to the orientations of each grain as indicated by the unit triangle in the figure. In Figs. 8(c, d), HAGBs with misorientation angles greater than 15° are represented by green lines, while LAGBs with misorientation angles of 2°−15° are indicated by red lines. It should also be noted that the uneven grain size distribution of the samples in this figure, especially for the ARB samples, may be attributed to the non-uniformity of the rolling deformation.

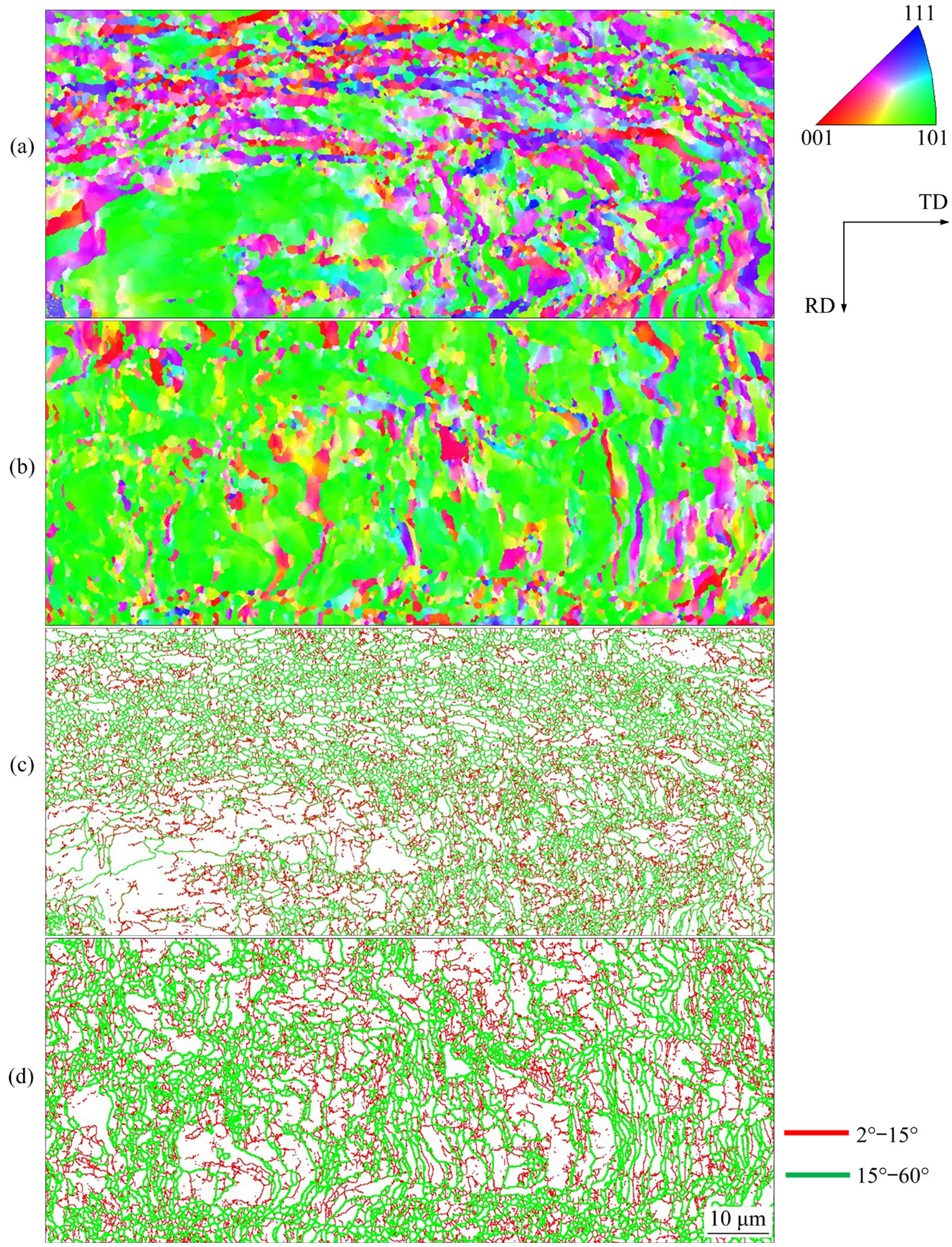

Fig. 8 Orientation (a, b) and grain boundary (c, d) maps of 7-cycle ARB (a, c) and 7-cycle CARB (b, d) specimens

According to the EBSD analysis, the misorientation angle distribution of the ARB and CARB samples is shown in Fig. 9. The fraction of HAGBs and the mean misorientation angle of the boundaries of the ARB sample are 45% and 20.38°, respectively, while those of the CARB sample are 48% and 23.32°, respectively. Obviously, compared with ARB, more grain boundaries in 6061 Al become high-angle boundaries after CARB.

Figure 10 shows the grain size diagrams of the 7-cycle ARB and CARB samples. The grain size distribution of 6061 Al after ARB and CARB is mainly concentrated in the range of 0−2 μm, with ultrafine grains of 0−0.5 μm dominating, accounting for about 68%. Similar to ARB, the CARB sample has 77% of the grains smaller than 500 nm. The average grain size of the starting material is known to be about 24 μm. Consequently, after 6061 Al is subjected ARB and CARB, many large grains are refined into small grains, and the grains are smaller under CARB.

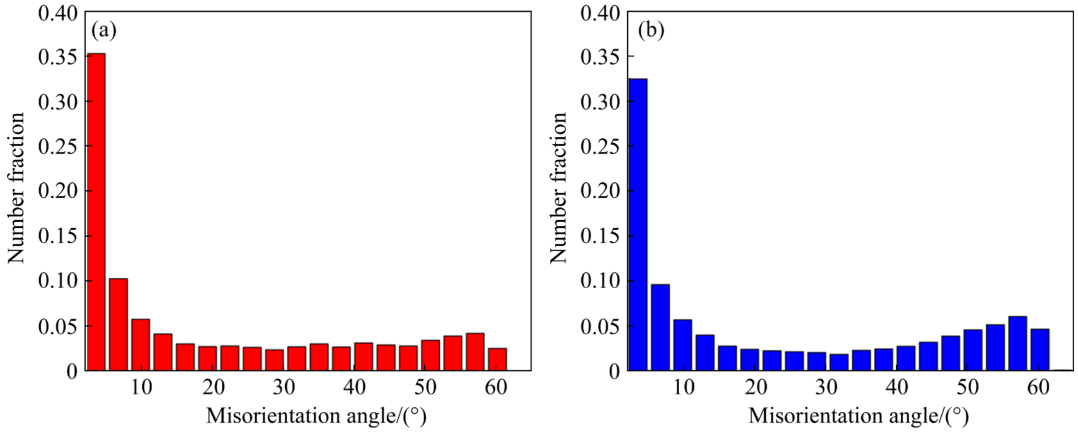

Fig. 9 Misorientation angle distributions of 7-cycle ARB (a) and 7-cycle CARB (b) specimens

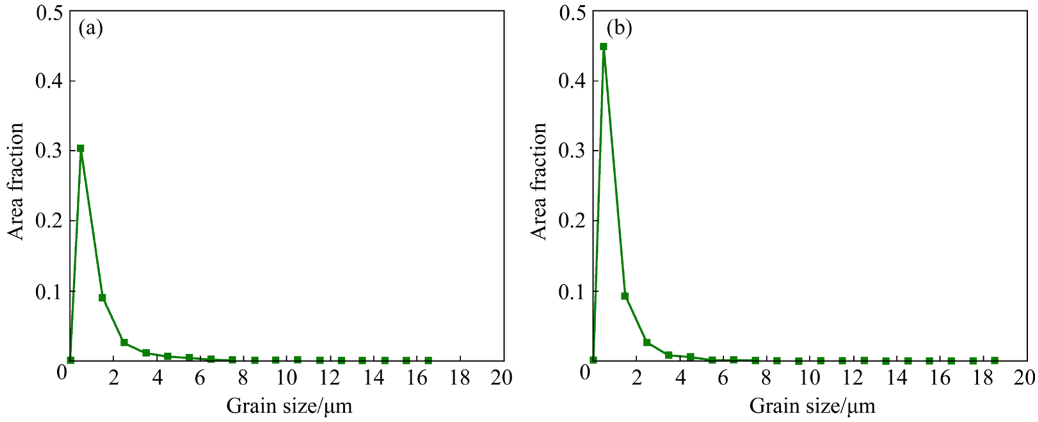

Fig. 10 Grain size distributions of 7-cycle ARB (a) and 7-cycle CARB (b) specimens

3.2.3 TEM result

Figure 11 shows TEM images, corresponding selected area diffraction (SAD) patterns and grain size distributions of 7-cycle ARB and CARB samples. As shown in Fig. 11(a), the microstructure of the rolled material changes into an ultrafine-grained laminate structure. After ARB processing, the average grain width is refined to 176 nm. The SAD pattern shows complex shape. This means that the grains formed in the specimen have some misorientations to each other. After CARB processing, the average grain width is refined to 75 nm. The average grain size of the samples processed by CARB is smaller than that of ARB. In general, the strength of ultrafine-grained materials increases with decreasing grain size. This is in good agreement with the results of the tensile properties of the rolled material.

Figure 12 shows TEM images, and corresponding SAD patterns (inset in Figs. 12(a, d)) with zone axis [110] for the 7-cycle ARB and CARB samples. It can be seen from Figs. 12(a, d) that there are a large number of widely distributed dislocation structures in samples. Dislocations are intensified during movement of dislocations, resulting in fixed dislocation jog or dislocation tangle. Tangles of dislocations can lead to the appearance of dislocation walls and dislocation lines, which in turn divide larger grains and promote the formation of subgrains.

Figures 12(b, e) show HRTEM images and corresponding SAD pattern with zone axis [110] for the 7-cycle ARB and CARB samples. Figures 12(c, f) show inverse fast Fourier transform (IFFT) images from the dash line frame in Figs. 12(b, e). The high density of dislocations can be seen in the IFFT images. The local dislocation density of CARB in Fig. 12(f) is as high as 9.89×10^{16} m^{-2}, which is higher than that of ARB (5.24×10^{16} m^{-2}). Most of the dislocations usually appear as dipoles (solid ellipses in Figs. 12(c, f)) with opposite Burgers vectors. These dipoles are caused by the local stress concentration during the ARB and CARB process.

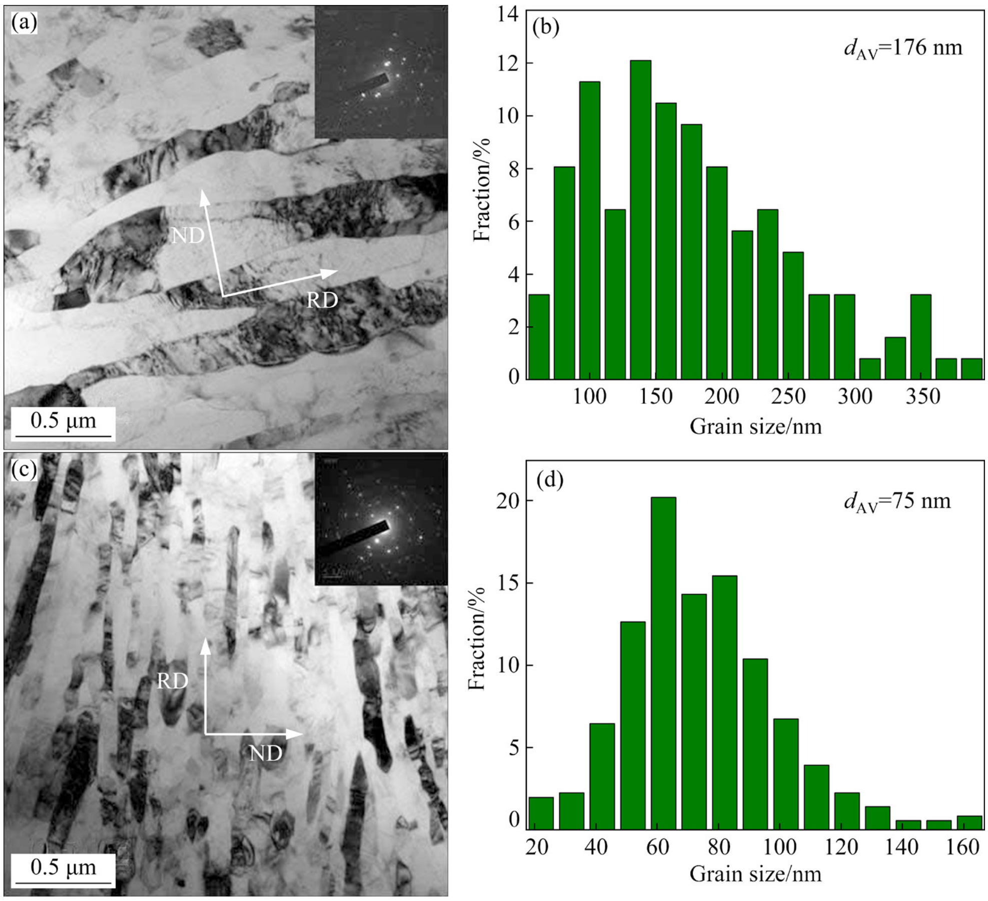

Fig. 11 TEM images, corresponding SAD patterns (a, c) and grain size distributions (b, d) of samples: (a, b) 7-cycle ARB; (c, d) 7-cycle CARB

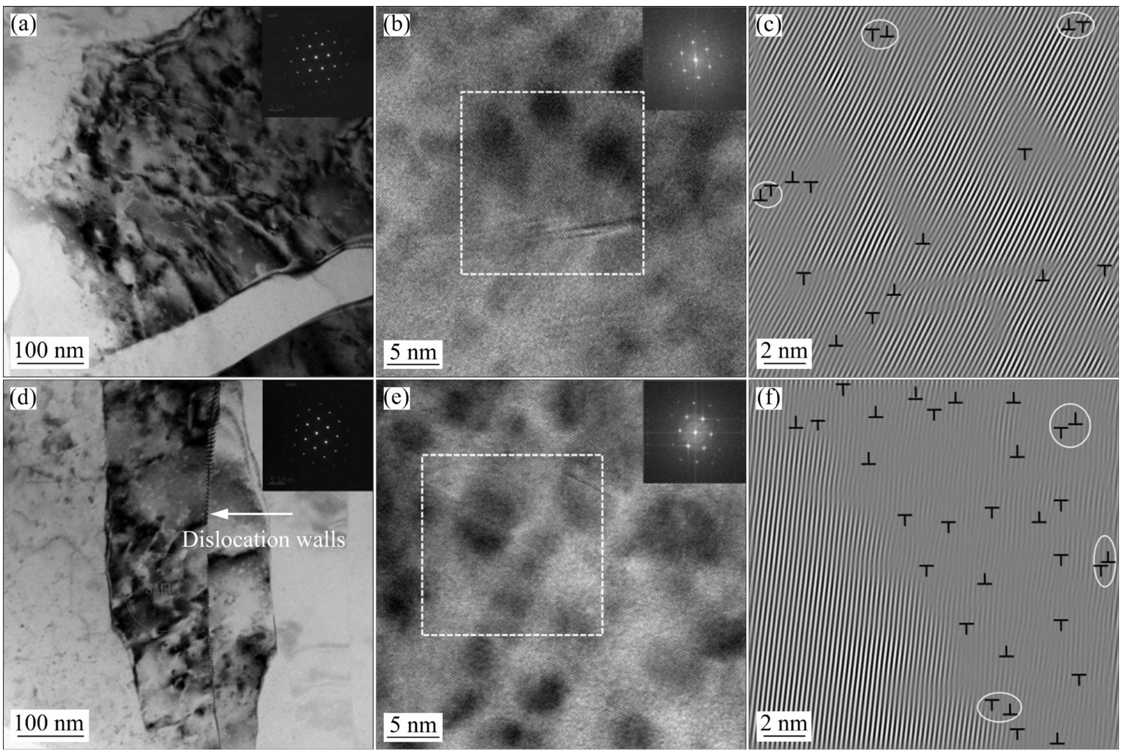

Fig. 12 TEM images (a, d), HRTEM images (b, e) and IFFT images (c, f) of samples: (a−c) 7-cycle ARB; (d−f) 7-cycle CARB

4 Discussion

4.1 Strengthening mechanisms

It can be seen from Fig. 3 that the surface microhardness of the 6061Al sheets increases with increasing the number of cycles. This trend is consistent with the experimental results obtained by REZAEI et al [8]. LEE et al [14] have investigated that the ultimate tensile strength of the 8-cycle ARB 6061 alloy sample is 363 MPa. YU et al [15] and REZAEI et al [8] have investigated that the ultimate tensile strength of the 5-cycle ARB 6061 alloy sample are 380 MPa and 362.5 MPa, respectively. In contrast, the performance data obtained by CARB in this experiment is better, and the ultimate tensile strength of the 7-cycle sample is 458 MPa. During the ARB process, the strength of 6061 Al sheet is mainly affected by the two mechanisms of dislocation strengthening and fine grain strengthening. The main reason of fine grain strengthening lies in the hindering effect of dislocations among grain boundaries. A fine-grained material has a greater total grain boundary area to impede dislocation motion than a coarse grained material [16].

The strengthening effect of dislocations in the alloy can be calculated according to Taylor's formula [17]:

$$\Delta\sigma_{\mathrm{d}}=M\alpha Gb\rho^{1/2} \tag{1}$$

where $\Delta\sigma_{\mathrm{d}}$ is the increase in yield strength caused by dislocations, M is the Taylor factor, α is a constant, G is the shear modulus, b is the magnitude of Burger vector, and ρ is the dislocation density. It can be seen that the strength of the materials increases with the increase of the dislocation densities.

From Fig. 3, the microhardness of the ARB and CARB samples increases with increasing the number of cycles. The main reason for the deformation of the plate is the movement of intragranular dislocations, which causes the dislocation densities and deformation resistance in the plate to increase. The effect of work hardening is obvious, and the hardness of the material is obviously improved. As shown in Fig. 3, each cycle of the CARB samples has higher microhardness than that of ARB. This is because the material rotates along the ND from the second cycle of CARB. Due to the change of the strain path, higher dislocation densities can be achieved. In Fig. 12, there are a large number of widely distributed dislocation structures in the 7-cycle ARB and CARB samples, which is beneficial to improving the strength of the alloy. The measured dislocation density of the CARB sample is $9.89\times10^{16}\,\mathrm{m}^{-2}$, significantly higher than that of ARB, which is beneficial to improving the strength of the alloy. It is well known that plastic deformation in one direction in metals affects the subsequent plastic response in the other direction. The effect of strain path changes on the mechanical properties of metal materials by SPD was investigated [18,19]. The difference in slip activity during the change of the ECAP strain path can activate the new slip system, thereby increasing the dislocation densities at the dislocation boundary [20]. The accumulation of excess dislocations in the geometrically-necessary interface increases the difference in crystal orientation, thereby increasing the rate of sub-micron grain formation.

According to the EBSD analysis, the fraction of HAGBs and the mean misorientation angle of boundaries of the ARB sample are 45% and 20.38°, respectively, while those of the CARB sample are 48% and 23.32°, respectively. Under large strain, many geometric dislocation boundaries evolve into HAGBs. Compared with ARB, more grain boundaries transform into HAGBs in 6061 Al processed by CARB, and many large grains are refined into ultrafine grains. In addition, the TEM results also show that the average grain width of sample processed by 7-cycle ARB is refined to 176 nm, while that of the CARB sample is 75 nm. The average grain size of the CARB sample is smaller than that of the ARB sample. The comprehensive results of the two experiments show that the material is basically composed of fine ultrafine grains at this stage, and the fine grain strengthening effect is remarkable. A study [21] has shown that under higher rolling cycles, it is difficult to accumulate dislocations, and the performance of the material at this time is mainly controlled by the gradual evolution of ultrafine grains. The gradual formation of ultrafine grains plays a major role in strengthening.

The grain refinement of 6061 Al sheet processed by high-cycle accumulative rolling is also related to the change of texture orientation density. The formation of rolling textures for face-centered cubic (fcc) metals by a rate dependent crystal plasticity model was investigated in literatures [22,23]. During deformation, the ideal texture moves either directly into the α-fiber or the β-fiber and finally towards the corresponding stable components. During the ARB process, plane strain deformation of fcc metals causes orientations to concentrate along the α-fiber and β-fiber. The textural components of the samples subjected to ARB can be characterized as Copper $\{112\}\langle 111\rangle$, S $\{123\}\langle 634\rangle$, and Brass $\{011\}\langle 211\rangle$. In addition, there are some Goss $\{011\}\langle 100\rangle$ textures. The 7-cycle ARB sample has a strong orientation density and uniform distribution on the β-fiber. In contrast, due to the change of the rolling path, the Copper $\{112\}\langle 111\rangle$ and S $\{123\}\langle 634\rangle$ rolling texture components of the CARB sample are significantly weakened, and the β-fiber is mainly concentrated on Brass $\{011\}\langle 211\rangle$ texture. In the ARB process, the division of grains by deformation bands leads to the dispersion of ideal texture components, and the formation of strong textures leads to the formation of band-like structures and prevents the complete refinement of sub-micron grains [24]. Compared with ARB, the texture components of the CARB sample are weakened, which is conducive to grain refinement.

4.2 Tensile plasticity

In general, the elongation of the materials shows a downward trend with increasing the number of ARB cycles, because the inherent microstructure and deformation mechanism of the materials are related to their own low strain hardening ability after ARB. With increasing the number of cycles, the strain hardening ability gradually weakens, resulting in poor plasticity.

The change of the dislocation densities of the ARB material during the stretching process plays a key role in the tensile plasticity of the materials. The grain size of the material processed by ARB is small, and the higher-cycle material has an ultra-fine crystal structure. During the stretching process, two situations occur at the same time. The first is that new dislocations are generated at the grain boundaries, which are combined with the original dislocations to form dislocation entanglements, and the dislocation density increases, thereby improving the work hardening ability. Secondly, the original dislocations are annihilated and rearranged, the dislocation density is reduced, and the work hardening ability is reduced. If the material has a higher dislocation density prior to stretching, the effect of the first case is less than that of the second case, corresponding to a low work hardening rate. On the contrary, it shows a high work hardening rate. In terms of dislocation density, the ARB and CARB samples have a higher dislocation density than the solution treated specimen. In other words, the rolled material should all have lower tensile ductility. LEE et al [14] have examined that the elongation of the 8-cycle ARB 6061 Al alloy sample is 5%. YU et al [15] and REZAEI et al [8] have studied that the elongation of the 5-cycle ARB 6061 Al alloy sample is 3% and 4%, respectively. In contrast, the performance data obtained by CARB in this experiment are better, and the elongation of the 7-pass sample is 12.1%. It can be seen from Fig. 4 that the elongation of CARB 6061 Al sheet is significantly higher than that of ARB, and the elongation increases by 22.2%. The increase in ductility can be explained by the formation of ultra-fine grains and control of texture [25,26].

During the CARB process, the 6061 Al plate is continuously rotated by 90° around the rolling direction. The layer boundary of the plate in the rolling channel is also alternatively parallel or perpendicular in different rolling cycles, which greatly reduces the length-to-diameter ratio between the connection boundary spacing and the lamella boundary spacing, improves the grain refinement efficiency, and thereby enhances the grain refinement strengthening effect of 6061 Al alloy. HOU et al [27] revealed that fine grains are very beneficial to improving the compatibility among the grains, so that high ductility can be achieved. Some literature reports that the HAGBs in the fine grains are the main reason for the enhanced ductility, because the HAGBs can effectively enhance the dislocation accumulation to increase the work hardening rate [28]. Compared with coarse-grained homogenized alloys, ultrafine grained alloys have a higher work hardening rate, indicating that grain refinement plays an important role in increasing the work hardening rate. A large number of ultrafine grains or grain boundaries can effectively prevent the movement of dislocations, thereby increasing the work hardening rate. The higher the proportion of ultrafine grains is, the higher the work hardening rate is. CARB material with a smaller average grain width obtains finer ultrafine grains than ARB so that the strength is further improved while maintaining good plasticity. Therefore, the change in rolling path makes the CARB material stronger and better than ARB, which is also confirmed by the tensile fracture morphologies.

During the CARB process, the cross-rolling behavior causes the sheet to have a weak texture. The weakening of the substrate texture is very conducive to improving the ductility of material, because the slip is easily activated [29]. XIAO et al [26] revealed that the transition from a strong deformed texture to a weak recrystallized texture has an important contribution to the improvement of elongation. Higher tensile strains can be obtained because the randomly oriented fine grains facilitate uniform stress distribution, which greatly reduces local deformation during the tensile deformation process.

In summary, the higher ductility of 6061 Al alloy processed by CARB is mainly due to the finer grains and weak texture. The high proportion of HAGBs in CARB can increase the work hardening rate by effectively preventing the movement of dislocations. The weak texture can effectively reduce the stress concentration.

5 Conclusions

(1) The UTS of the 7-cycle CARB sample is 458 MPa and the elongation is 12.1%. Compared with ARB, the UTS of the CARB sample increases by 11.2% and the elongation increases by 22.2%.

(2) The grains on RD−TD planes that are smaller than 500 nm account for 68% and 77% in ARB and CARB samples, respectively. The average grain size of samples on the RD−ND planes processed by 7-cycle ARB is refined to 176 nm, while that of the 7-cycle CARB sample is 75 nm. The average grain size of the CARB samples is smaller than that of ARB.

(3) The local dislocation density of CARB is as high as $9.89\times10^{16}\,m^{-2}$, which is significantly larger than that of ARB.

(4) The textural components of the ARB can be characterized as Copper $\{112\}\langle111\rangle$, S $\{123\}$-$\langle634\rangle$, and Brass $\{011\}\langle211\rangle$. In contrast, the rolling textures of the 6061 alloy materials processed by CARB are significantly weakened.

(5) The high strength of CARB 6061 Al alloy is mainly dominated by ultrafine grains and dislocation strengthening, and higher strength is achieved by grain refinement with finer grains and higher dislocation density. The higher ductility of CARB sheet is mainly attributed to finer grains and weak texture.

Acknowledgments

The authors are grateful for the financial supports from the National Natural Science Foundation of China (No. 52271177), the Scientific Research and Innovation Foundation of Hunan University of Technology, China (No. CX2210), the Natural Science Foundation of Hunan Province, China (No. 2023JJ50181), the Major Special Projects in Anhui Province, China (No. 202003c08020005), and the Science and Technology Innovation Leaders Projects in Hunan Province, China (No. 2021RC4036).

References

[1] SAITO Y, TSUJI N, UTSUNOMIYA H, SAKAI T, HONG R G. Ultra-fine grained bulk aluminum produced by accumulative roll-bonding (ARB) process [J]. Scripta Materialia, 1998, 39(9): 1221−1227.

[2] DEHGHAN M, QODS F, GERDOOEI M, MOHAMMADIAN-SEMNANI H. Effect of inter-cycle heat treatment in accumulative roll-bonding (ARB) process on planar isotropy of mechanical properties of AA1050 sheets [J]. Transactions of Nonferrous Metals Society of China, 2020, 30(9): 2381−2393.

[3] DU Qing-lin, LI Chang, CUI Xiao-hui, KONG Charlie, YU Hai-liang. Fabrication of ultrafine-grained AA1060 sheets via accumulative roll bonding with subsequent cryorolling [J]. Transactions of Nonferrous Metals Society of China, 2021, 31(11): 3370−3379.

[4] SEIFOLLAHZADEH P, ALIZADEH M, ABBASI M R. Strength prediction of multi-layered copper-based composites fabricated by accumulative roll bonding [J]. Transactions of Nonferrous Metals Society of China, 2021, 31(6): 1729−1739.

[5] WANG Lin, DU Qing-lin, LI Chang, CUI Xiao-hui, ZHAO Xiao, YU Hai-liang. Enhanced mechanical properties of

lamellar Cu/Al composites processed via high-temperature accumulative roll bonding [J]. Transactions of Nonferrous Metals Society of China, 2019, 29(8): 1621−1630.

[6] ZHONG F, WANG T Z, WU R Z, HOU L G, ZHANG J H, LI X L, ZHANG M L, DONG A P, SUN B D. Microstructure, texture, and mechanical properties of alternate α/β Mg−Li composite sheets prepared by accumulative roll bonding [J]. Advanced Engineering Materials, 2017, 19(5): 1600817.

[7] CHANG H, ZHENG M Y, GAN W M, WU K, MAAWAD E, BROKMEIER H G. Texture evolution of the Mg/Al laminated composite fabricated by the accumulative roll bonding [J]. Scripta Materialia, 2009, 61(7): 717−720.

[8] REZAEI M R, TOROGHINEJAD M R, ASHRAFIZADEH F. Effects of ARB and ageing processes on mechanical properties and microstructure of 6061 aluminum alloy [J]. Journal of Materials Processing Technology, 2011, 211(6): 1184−1190.

[9] KHATAMI R, FATTAH-ALHOSSEINI A, MAZAHERI Y, KESHAVARZ M K, HAGHSHENAS M. Microstructural evolution and mechanical properties of ultrafine grained AA2024 processed by accumulative roll bonding [J]. The International Journal of Advanced Manufacturing Technology, 2017, 93(1/2/3/4): 681−689.

[10] LI Lin-yan, OU Ling, FAN Cai-he, YANG Jian-jun, YUAN Shu-wen, CHEN Pei-lin. Research progress of accumulative roll bonding [J]. Packaging Journal, 2021, 13(4): 8. (in Chinese)

[11] LI X Y, XIA W J, YAN H G, CHEN J H, SU B, SONG M, LI Z Z, LU Y. High strength and large ductility of a fine-grained Al−Mg alloy processed by high strain rate hot rolling and cold rolling [J]. Materials Science and Engineering A, 2020, 787: 139481.

[12] NASERI M, REIHANIAN M, BORHANI E. A new strategy to simultaneous increase in the strength and ductility of AA2024 alloy via accumulative roll bonding (ARB) [J]. Materials Science and Engineering A, 2016, 656: 12−20.

[13] NASERI M, REIHANIAN M, BORHANI E. Effect of strain path on microstructure, deformation texture and mechanical properties of nano/ultrafine grained AA1050 processed by accumulative roll bonding (ARB) [J]. Materials Science and Engineering A, 2016, 673: 288−298.

[14] LEE S H, SAITO Y, SAKAI T, UTSUNOMIYA H. Microstructures and mechanical properties of 6061 aluminum alloy processed by accumulative roll-bonding[J]. Materials Science and Engineering A, 2002, 325: 228−235.

[15] YU H L, SU L H, LU C, TIEU K, LI H J, LI J T, GODBOLE A, KONG C. Enhanced mechanical properties of ARB-processed aluminum alloy 6061 sheets by subsequent asymmetric cryorolling and ageing [J]. Materials Science and Engineering A, 2016, 674: 256−261.

[16] NARUTANI T, TAKAMURA J. Grain-size strengthening in terms of dislocation density measured by resistivity [J]. Acta Metallurgica et Materialia, 1991, 39(8): 2037−2049.

[17] PARK J M, YANG D C, KIM H J, KIM D G, LEE S, KIM H S, SOHN SS. Ultra-strong and strain-hardenable ultrafine-grained medium-entropy alloy via enhanced grain-boundary strengthening [J]. Materials Research Letters, 2021, 9(7): 315−321.

[18] IWAHASHI Y, HORITA Z, NEMOTO M, LANGDON T G. The process of grain refinement in equal-channel angular pressing[J]. Acta Materialia, 1998, 46: 3317−3331.

[19] LI S Y. Dependencies of grain refinement on processing route and die angle in equal channel angular extrusion of bcc materials [J]. Computational Materials Science, 2009, 46(4): 1044−1050.

[20] CABIBBO M. A TEM Kikuchi pattern study of ECAP AA1200 via routes A, C, BC [J]. Materials Characterization, 2010, 61(6): 613−625.

[21] LI B L, TSUJI N, KAMIKAWA N. Microstructure homogeneity in various metallic materials heavily deformed by accumulative roll-bonding [J]. Materials Science and Engineering A, 2006, 423: 331−342.

[22] CHOWDHURY S G, SRIVASTAVA V C, RAVIKUMAR B, SOREN S. Evolution of texture during accumulative roll bonding (ARB) and its comparison with normal cold rolled aluminium–manganese alloy [J]. Scripta Materialia, 2006, 54(9): 1691−1696.

[23] SU L, LU C, GAZDER A A, SALEH A A, DENG G, TIEU K, LI H. Shear texture gradient in AA6061 aluminum alloy processed by accumulative roll bonding with high roll roughness [J]. Journal of Alloys and Compounds, 2014, 594: 12−22.

[24] PASEBANI S, TOROGHINEJAD M R, HOSSEINI M, SZPUNAR J. Textural evolution of nano-grained 70/30 brass produced by accumulative roll-bonding [J]. Materials Science and Engineering A, 2010, 527: 2050−2056.

[25] ZHA Min, ZHANG Hong-min, YU Zhi-yuan, ZHANG Xuan-he, MENG Xiang-tao. Bimodal microstructure-A feasible strategy for high-strength and ductile metallic materials [J]. Journal of Materials Science & Technology, 2018, 34(2): 15−22.

[26] XIAO H, LU Z, ZHANG K F, JIANG S S, SHI C C. Achieving outstanding combination of strength and ductility of the Al−Mg−Li alloy by cold rolling combined with electropulsing assisted treatment [J]. Materials & Design, 2020, 186: 108279.

[27] HUO W T, SHI J T, HOU L G, ZHANG J S. An improved thermo-mechanical treatment of high-strength Al−Zn−Mg−Cu alloy for effective grain refinement and ductility modification [J]. Journal of Materials Processing Technology, 2017, 239: 303−314.

[28] WU J, CHEN J H, YAN H G, XIA W J, SU B, YU L, LIU G S, SONG M. Enhancing the mechanical properties of high strain rate rolled Mg−6Zn−1Mn alloy by pre-rolling [J]. Journal of Materials Science, 2017, 52: 10557−10566.

[29] SABAT R K, BRAHME A P, MISHRA R K, INAL K, SUWAS S. Ductility enhancement in Mg−0.2%Ce alloys [J]. Acta Materialia, 2018, 161: 246−257.

交叉累积叠轧法制备高强高韧 6061 铝合金

欧 玲[1]，李林艳[1]，范才河[1,2]，聂宇峰[3]，阳建君[1]

1. 湖南工业大学 材料与先进制造学院，株洲 412007；
2. 安徽建业科技有限公司，淮北 235000；
3. 湖南工业大学 机械工程学院，株洲 412007

摘 要：为了实现强度与塑性的良好匹配，在室温下采用交叉累积叠轧(CARB)技术制备 7 道次 6061 铝合金薄板。利用 X 射线衍射、透射电子显微镜、扫描电子显微镜和电子背散射衍射对其微观结构进行分析。结果表明：CARB 试样的极限抗拉强度和伸长率均明显优于 ARB 试样。CARB 试样的平均晶粒尺寸更小，有更多的小角度晶界转变成大角度晶界，且位错密度更高。CARB 制备出的 6061 合金材料轧制织构明显弱化，以 Brass{011}⟨211⟩织构为主。CARB6061 合金的更高强度主要由超细晶粒强化和位错强化导致，更高延展性归因于更细小的晶粒和弱织构。

关键词：交叉累积叠轧；6061 铝合金；电子背散射衍射；晶体学织构；拉伸力学性能

(Edited by Bing YANG)